DRAPER, N. R. & SMITH, H. (1981). *Applied Regression Analysis*, 2nd ed. New York: Wiley.
FUJINO, K., SASAKI, S., TAKEUCHI, Y. & SADANAGA, S. (1981). *Acta Cryst.* B37, 513–518.
GERR, R. G., BOROVSKAYA, T. N., VOLOSHINA, I. V., LOBANOV, N. N., SLOVOKHOTOVA, O. L., STRELTSOV, V. A., STRUCHKOV, Y. T., OZEROV, R. P., TSIRELSON, V. G. & YANOVSKII, A. I. (1991). *J. Struct. Chem.* Submitted.
HANSEN, N. K. (1991). In *Logiciels pour la Chimie – Catalogue de Logiciels de Recherche*, edited by La Société de Chimie Française, Paris.
HANSEN, N. K. & COPPENS, P. (1978). *Acta Cryst.* A34, 909–921.
HANSEN, N. K., PROTAS, J. & MARNIER, G. (1991). *Acta Cryst.* B47, 660–672.
HOLLADAY, A., LEUNG, P. & COPPENS, P. (1983). *Acta Cryst.* A39, 377–387.
JOHNSON, C. K. (1965). *ORTEP*. Report ORNL-3794. Oak Ridge National Laboratory, Tennessee, USA.
KURKI-SUONIO, K. (1977). *Isr. J. Chem.* **16**, 115–123.
LARSON, A. C. (1970). In *Crystallographic Computing*, edited by F. R. AHMED. Copenhagen: Munksgaard.
SANTORO, R. P. & NEWNHAM, R. E. (1967). *Acta Cryst.* **22**, 344–347.
STRELTSOV, V. A., TSIRELSON, V. G. & OZEROV, R. P. (1990). In *Problems of Crystal Chemistry*, edited by M. A. PORAI-KOSHITS. Moscow: Nauka. (In Russian.)
TSIRELSON, V. G., STRELTSOV, V. A., OZEROV, R. P. & IVON, K. (1989). *Phys. Status Solidi A*, **115**, 515–521.
YAKUBOVICH, O. V., BELOKONEVA, E. L., TSIRELSON, V. G. & URUSOV, V. S. (1990). *Vestnik Moscow Univ.* **4**, 99–105. (In Russian.)
YAKUBOVICH, O. V., SIMONOV, M. A. & BELOV, N. V. (1977). *Sov. Phys. Dokl.* **22**, 347–348.

Acta Cryst. (1993). B49, 153–158

Maximum Entropy as a Tool for the Determination of the *c*-Axis Profile of Layered Compounds

BY PH. DEPONDT

Département de Recherches Physiques (URA CNRS 71), Université Pierre et Marie Curie, 75252 Paris CEDEX 05, France

D. A. NEUMANN

Reactor Radiation Division, National Institute of Standards and Technology, Gaithersburg, MD 20899, USA

AND S. F. TREVINO

ARDEC, Picatinney Arsenal, NJ, USA, and Reactor Radiation Division, National Insitute of Standards and Technology, Gaithersburg, MD 20899, USA

(*Received* 15 *June* 1992; *accepted* 29 *October* 1992)

Abstract

A simple procedure for the determination of the structure normal to the basal plane of layered compounds based on the now ubiquitous maximum-entropy method is presented. It is illustrated by the analysis of room-temperature (00*l*) elastic neutron-scattering experiments performed on two graphite intercalation compounds, stage 3 $C_{44.6}MoCl_5$ and stage 1 $KC_{24}(ND_3)_{4.3}$. The former example is quite simple, requiring only a crude heuristic model to determine the structure-factor phases. The latter shows good sensitivity to the orientation of the ND_3 threefold axis with respect to the basal plane, thus providing its first direct determination.

1. Introduction

The properties of many layered materials, such as graphite, transition-metal dichalcogenides and layer silicates, can be substantially altered by the intercalation of various guest species into the interlayer region (gallery) of the host. Because of the lack of single crystals and the prevalance of stacking faults, complete structural determinations of these systems are seldom made. However, owing to the 'platelike' nature of the individual pieces, it is often possible to fabricate oriented specimens in which the *c* axes (*i.e.* the direction perpendicular to the basal planes) of the pieces are well aligned, but the in-plane crystallographic axes are not. One can then use X-ray or neutron scattering to obtain scans along the **c** direction – (00*l*) scans – which reflect important structural information in these materials, such as the distance between guest and host layers, the guest density within the galleries, the orientation of polyatomic guests and, for graphite intercalation compounds, the stage. Furthermore, because of the complicated phase diagrams of these materials, such information is required before any meaningful interpretation of other data can be made. Thus, one requires a method

0108-7681/93/020153-06$06.00

by which this information can be obtained quickly and reliably. Since this problem is one dimensional, the maximum-entropy method (MEM) (Jaynes, 1957) provides such a method. While the MEM is often associated with large and complex computations (Bricogne, 1984), this is certainly not the case when determining the c-axis structure of layered compounds. Rather one simply uses the MEM in conjunction with a rather crude model as opposed to least-squares fitting procedures for which one has to be reasonably realistic. Here we illustrate the application of this method with two rather different examples, stage 3 $MoCl_5$ intercalated graphite and stage 1 $K(ND_3)_{4.3}$ intercalated graphite.

A number of experiments (Suzuki, Furukawa, Ikeda & Nagano, 1983; Suzuki, Santodonato, Suzuki, White & Cotts, 1991) have shown that $MoCl_5$-intercalated graphite undergoes various phase transitions one of which takes place at $T_c = 480$ K in the stage 3 compound and shows a λ-type anomaly. The $MoCl_5$ intercalated layers are uncorrelated with respect to one another. Our interest presently resides mainly in the fact that it is a fairly simple example for the MEM.

Alternatively, X-ray (Qian, Stump, York & Solin, 1985; Qian, Stump & Solin, 1986) and neutron (Fan, Solin, Neumann, Zabel & Rush, 1987) scattering experiments have shown that the potassium–ammonia layer in the stage 1 graphite intercalation compound $KC_{24}(ND_3)_{4.3}$ is a two-dimensional liquid at room temperature. The in-plane structure of the intercalate layer displays loosely bound planar $K(ND_3)_4$ molecular complexes, while the remaining ammonia molecules are essentially free. In addition, a quasi-elastic neutron-scattering study (Neumann, Zabel, Rush, Fan & Solin, 1987) indicates that, in the protonated compound, the NH_3 threefold axis lies parallel to the carbon plane. It is, however, essential to obtain a clearer view of the orientational distribution of the ammonia C_3 axis, since an inelastic scattering experiment (Neumann, Zabel, Fan, Solin & Rush, 1988) shows that the (00l) longitudinal phonons couple to a libration of the ammonia molecule, the exact nature of which remains to be understood.

The experimental aspects are discussed in §2, while §3 provides a brief reminder of the method and its adaptation to our specific problem.* Results are summarized in §4.

2. Experimental

Table 1 shows the integrated intensities of the (00l) peaks obtained at room temperature using the BT4 triple-axis spectrometer at the Neutron-Beam Split-Core Reactor at NIST. A Cu (220) monochromator was used to obtain an incident energy of 150 meV. No analyser was used. The relatively large energy was necessary to reach the large wavevector at which the $l = 17$ reflection in the first case, and the $l = 11$ reflection in the second could be measured. The integrated intensities were obtained by fitting the individual peaks to Gaussian line shapes, and δ_l is the statistical uncertainty obtained *via* this procedure.

Table 1. *Integrated intensities and uncertainties after subtraction of background and sample can contributions*

	$C_{44.6}MoCl_5$		$KC_{24}(ND_3)_{4.33}$	
l	I_l	δ_l	I_l	δ_l
1	672	9	200	3
2	79	3	2413	11
3	97	13	430	6
4	1618	4	492	6
5	3298	70	317	5
6	19	7	300	3
7	21	12	84.9	3.4
8	0	7	205	6
9	1322	44	58.7	3.9
10	1387	45	135	16
11	21	7	60	16
12	6	5		
13	17	7		
14	741	33		
15	207	18		
16	15	9		
17	0	9		

In the case of $MoCl_5$ a least-squares fit of a model to these results is feasible, and indeed the X-ray data (Suzuki *et al.*, 1991) were thus interpreted, but we want to address this problem as if we were in a situation in which we needed to do a quick structure determination with as few *a priori* assumptions as possible.

In the case of potassium–ammonia intercalated graphite, on the other hand, a model suitable for a least-squares fit analysis would require almost as many parameters as data. This is a good candidate for the maximum-entropy method since it determines the most likely solution, rather than a unique one.

3. The method

The result of a neutron elastic scattering experiment can be expressed as

$$F_l = C\sum_{\mu}\int_0^{c/2} n_\mu b_\mu p_\mu(z)\varepsilon_l \cos q_l z \mathrm{d}z \qquad (1)$$

where F_l is the structure factor of the (00l) peak, $q_l = 2\pi l/c$, with c being the lattice constant, $\varepsilon_l = \pm 1$ stands for a phase factor in a centrosymmetric system, b_μ is the scattering length of atom of type μ, n_μ is the number of atoms of type μ in the cell, $p_\mu(z)$ is the probability distribution function of an atom of type μ, and $C = 2F_0/\sum_\mu n_\mu b_\mu$ is a normalization constant.

* A good introduction to the maximum-entropy procedure is given by Frieden (1972).

In order to do numerical computations, the cell must be divided into pixels, and the integral in (1) replaced by a discrete sum, thus

$$F_l = C \sum_{i=1}^{\nu} \sum_{\mu} n_\mu b_\mu p_\mu(z_i) \varepsilon_l \cos q_l z_i \delta_z \qquad (2)$$

where δ_z is the size of a pixel, ν is the number of pixels and z_i is the coordinate of the middle of pixel i.

Let

$$\rho_i = \frac{\sum_\mu n_\mu b_\mu p_\mu(z_i) \nu \delta_z}{\sum_\mu n_\mu b_\mu} \qquad (3)$$

and

$$d_{il} = \frac{C \varepsilon_l \cos q_l z_i}{\nu}. \qquad (4)$$

Here ρ_i is the discretized nuclear density which is analogous to the electron density relevant to an X-ray experiment.

These definitions yield

$$F_l = \sum_{i=1}^{\nu} \rho_i d_{il} \qquad (5)$$

where $\{d_{il}\}$ is a set of known constants, and the unknown distribution $\{\rho_i\}$ is what we are seeking.

Obtaining the most likely set of $\{\rho_i\}$, the MEM (Jaynes, 1957; Frieden, 1972; Prince, 1989) requires maximizing the entropy S where

$$S = -\sum_i \rho_i \ln \rho_i \qquad (6)$$

given the constraints

$$F_l^{(\text{obs})} - \sigma_l \le F_l^{(\text{calc})} \le F_l^{(\text{obs})} + \sigma_l \qquad (7)$$

where $F_l^{(\text{calc})}$ is calculated from (5), $F_l^{(\text{obs})}$ is obtained from the experiment, and σ_l is the uncertainty.

This is a classical numerical problem of linearly constrained maximization, done by an iterative refinement of the Lagrange multipliers λ_l associated with the constraints,* where

$$\rho_i = \exp\left(\sum_l \lambda_l d_{il}\right) \text{ and } F_l^{(\text{calc})} = \sum_i d_{il} \exp\left(\sum_{l'} \lambda_{l'} d_{il'}\right). \qquad (8)$$

In that respect, the normalization condition, $\sum_{i=1}^{\nu} \rho_i = \nu$, which results from the definition of ρ_i in (3), is convenient as it allows, as a starting point, $\rho_i^{[0]} = 1$, $\forall i \in [1,\nu]$, which corresponds to all initial Lagrange multipliers $\lambda_l^{[0]}$, $\forall l \in [0,l_{\max}]$ set to 0. This normalization condition does not have to appear explicitly as a constraint, if $F_{l=0}$ is included, as it is implied by the definitions of C, ρ_i and d_{il}. At each iteration, the Lagrange multipliers are modified by a Newton–Raphsson linearization of $F_l^{(\text{calc})}$ with respect to λ_l. The differences $\delta F_l^{(\text{calc})[n+1]}$ which induce the variations $\delta\lambda_l^{[n+1]}$ for step $[n+1]$ are set by

$$\begin{aligned}
\delta F_l^{(\text{calc})[n+1]} &= F_l^{(\text{calc})[n]} - F_l^{(\text{obs})} - \sigma_l \\
&\quad \text{for } F_l^{(\text{calc})[n]} > F_l^{(\text{obs})} + \sigma_l, \\
\delta F_l^{(\text{calc})[n+1]} &= F_l^{(\text{calc})[n]} - F_l^{(\text{obs})} + \sigma_l \\
&\quad \text{for } F_l^{(\text{calc})[n]} < F_l^{(\text{obs})} - \sigma_l, \\
\delta F_l^{(\text{calc})[n+1]} &= 0 \\
&\quad \text{for } F_l^{(\text{obs})} - \sigma_l < F_l^{(\text{calc})[n]} < F_l^{(\text{obs})} + \sigma_l.
\end{aligned} \qquad (9)$$

Here, in the two first lines the constraints are *un*satisfied, whereas, in the third they are satisfied. This idea of (un)satisfied constraints, is crucial because if one maintains already satisfied constraints in the refinement procedure, it usually results in 'pulling' many of the calculated $F_l^{(\text{calc})}$ values much closer to the observed ones than warranted by error bars, thus creating great sensitivity to noise.* The procedure is stopped when all constraints are satisfied.

In order to be able to carry out this procedure, F_0 and ε_l need to be established, or at least estimated. This is done using a model which is only *heuristic*, and which can be therefore much cruder than one meant for a least-squares fit procedure. This is illustrated in the next section.

4. Results and discussion

$MoCl_5$-*GIC*

Fig. 1 displays $\rho(z)$ for $z = 0$ to $c/2$. Here the label 'Exp.' refers to the $\rho(z)$ obtained from the MEM using the data from Table 1, with $\varepsilon_l = +1\ \forall l \in [1,17]$ and $F_0 = 7000$ the smallest value for which the procedure would converge. Convergence is obtained in 18 steps (*ca* 5 s user time on a Gould NP1 with $\nu = 1000$). Three maxima occur at $z = 0$, $z \simeq 3.3$ and $z \simeq 6.6$ Å, with the third peak being rather ill defined. It is quite natural, therefore, to attribute the first and second peaks to carbon planes and the third to a chlorine plane. The molybdenum lies at $c/2 = 7.95$ Å. The symmetry with respect to $z = 0$ thus gives a total of three carbon planes betwen the intercalated galleries as expected for a stage 3 sample. The inclusion of a uniform translational disorder (Debye–Waller factor) of 0.3 Å provides the intensities given in Table 2, along with the signs of ε_l. The labels 'Calc.' and 'Exp., ε' shown in Fig. 1, refer to the $\rho(z)$

* Or any equivalent method, see *e.g.* Prince (1989).

* Frieden (1972) dealt with this problem differently by introducing noise explicity with what amounts to a statistical assumption that the mean noise is equal to zero. This is perfectly correct if, as in image-reconstruction problems, one is dealing with large quantities of experimental data, unfortunately not the case here.

Table 2. *Stage* 3 $MoCl_5$ (00*l*) *calculated intensities, uncertainties and* ε_l

l	I_l	δ_l	ε_l
0	395	11	1
1	9.00	0.39	1
2	0.747	0.041	−1
3	5.01	0.15	−1
4	47.3	1.6	1
5	265.8	7.5	1
6	0.400	0.036	1
7	0.444	0.033	−1
8	2.284	0.048	−1
9	53.3	1.6	1
10	108.2	3.1	1
11	1.0782	0.0082	−1
12	0.0124	0.0022	1
13	1.141	0.017	−1
14	35.4	1.0	1
15	18.76	0.56	1
16	0.3433	0.0055	−1
17	0.0225	0.0023	−1

obtained from these calculated intensities and ε_l, and on the experimental intensities with the same values of ε_l as in the calculated case, respectively. The improvement for the 'Exp., ε' case is clear. Four well defined peaks are observed at $z = 0$, $z = 3.3$, $z = 6.6$ and $z = 8$ Å with half-widths in the range 0.2–0.3 Å.

Fig. 2 compares the distribution $\rho(z)$ with that obtained after increasing the uncertainties δl by a factor of 4, *i.e.* after relaxing constraints. Note that the smaller peaks tend to decrease with increasing uncertainties. It should also be pointed out that the uncertainties as defined by the experiment are standard deviations estimated from the fit of a Gaussian function to the experimental profiles, whereas the maximum-entropy procedure considers the uncertainties as absolute boundaries, a much stricter requirement.

Fig. 3 compares $\rho(z)$, for $F_0 = 8000$, the smallest value for which the MEM procedure will converge with the set of ε_l given by the calculation, and for $F_0 = 12000$. The main features of the distribution remain unchanged, proving that this is not a crucial factor; in fact it can be considered as simply a contrast variation device.

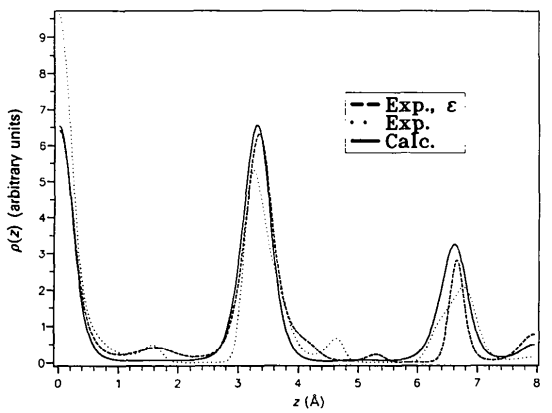

Fig. 1. Nuclear density $\rho(z)$ for stage 3 $MoCl_5$-GIC obtained by the MEM for the model described in the text (continuous line), the experiment assuming all structure factors are positive (dotted line) and the experiment using the structure-factor signs obtained from the model (dashed line).

$K(ND_3)_{4.3}$-*GIC*

Monte-Carlo integrations of (1) were performed with test probability distributions. The carbon, potassium and ammonia center of mass distributions were chosen as Gaussian, centered respectively at $z = 0$, $z = c/2$ and $z = c/2$ with half-widths set at 0.2 Å. The deuterium distribution around the ammonia threefold axis was chosen as isotropic, whereas θ, the angle between the **c** direction and the ND_3 axis was set first at 0, then 45 and 90° with half-width 10°. This was done for $l = 0$–11, thus providing an estimate for F_0 and showing that $\varepsilon_l = +1$, $\forall l \in [0,11]$. The computed structure factors were then fed into the MEM procedure in exactly the same way as the experimental data, thus yielding a total of four $\rho(z)$ distributions, one for each value of θ, and one for the experiment (Fig. 4). It was also checked that

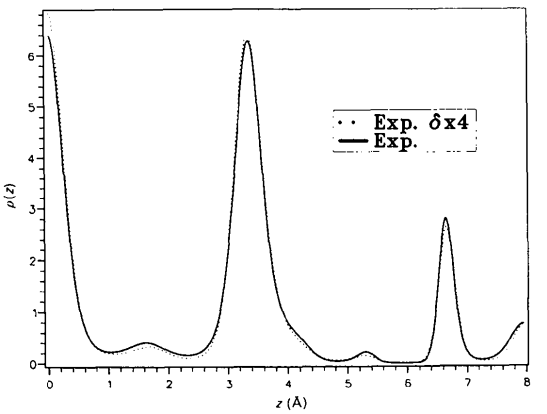

Fig. 2. Comparison of the results for $MoCl_5$ obtained with the experimental uncertainties δ (continuous line), and with these uncertainties multiplied by a factor of 4 (dotted line).

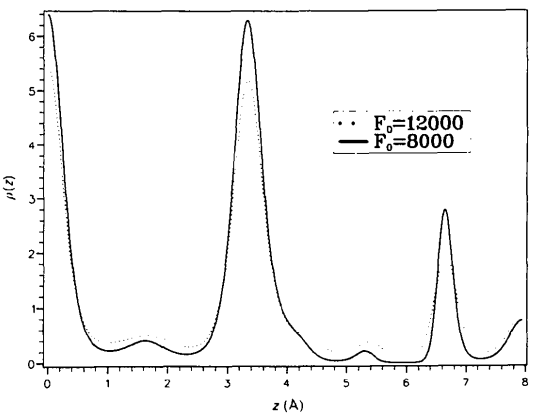

Fig. 3. Nuclear densities obtained for $MoCl_5$ for two values of F_0: 8000 (continous line) and 12000 (dotted line).

changing the estimate of F_0 for the experimental set within reasonable limits did not significantly alter the result (Fig. 5).

The computed distribution for $\theta = 90°$ displays a maximum at 2.5 Å corresponding to the width of the ammonia molecule (Fig. 6) whereas the broadening of the peak at 3.34 Å for $\theta = 0°$ is caused by the 'height' of the molecule. The large peak at $z = 0$ is the contribution from the carbon plane. The experimental result agrees most closely with the $\theta = 90°$ case, thus pointing to an ND_3 threefold axis lying in plane. At this point, questions may arise from the additional 'bump' at $z \simeq 0.75$ Å. Several $\rho(z)$ distributions were obtained using uncertainties δl which have been increased by factors of 2 and 4. As for the $MoCl_5$ case the small bumps disappear with increasing uncertainties. Again, this occurs because the δl values given in Table 1 are the statistical uncertainties obtained from a least-squares fitting procedure, but in the MEM they have been treated as absolute boundaries. Therefore, it is not unwarranted 'dabbling' with data to multiply these uncertainties by some factor but it is in fact necessary to do so in order to ascertain the reliability of any feature observed in the $\rho(z)$ obtained using this procedure.

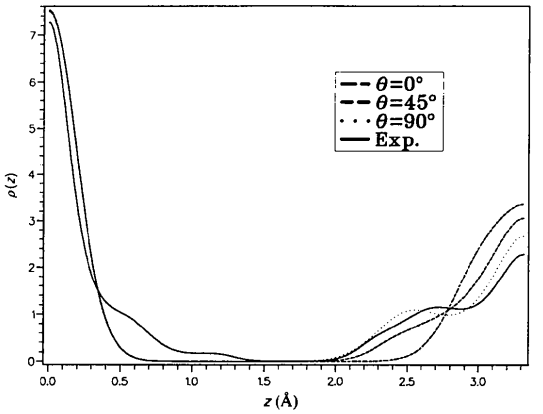

Fig. 4. Nuclear density $\rho(z)$ for stage 1 $K(ND_3)_{4.3}$-GIC obtained by the MEM for the experiment assuming all structure factors are positive (continuous line) and for the model with the ND_3 threefold axis lying in plane $\theta = 90°$ (dotted line), at a 45° angle (dashed line) and normal to the basal plane, $\theta = 0°$ (dot-dashed line).

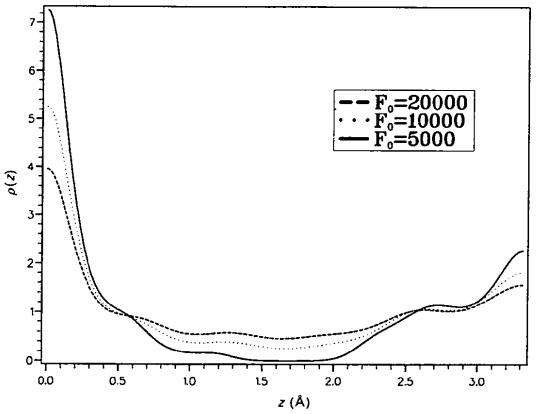

Fig. 5. Nuclear densities obtained for $K(ND_3)_{4.3}$ for three values of F_0: 5000 (continuous line), 10000 (dotted line) and 20000 (dashed line).

5. Concluding remarks

We have shown that the MEM provides a quick method to visualize in real space the results of diffraction experiments performed on layered materials yielding a good representation of the c-axis profile. The algorithm is universal, so that one does not have to write or modify computer programs for each new compound. The actual numbers obtained, such as the relative intensities of the real space peak or their widths, are rather reliable in spite of the fact that an experimental value of F_0, which has an influence on contrast, has not been determined. One should keep in mind, however, that here $\rho(z)$ has been obtained in the absence of any model. All that is required are the measured intensities of the (00l) reflections. When using a least-square fit, one must supply a physical model thereby adding considerable information to the experimental results. If the 'correct' model has been chosen, this additional information should result in more precise results than those obtained using the MEM.

More specifically, this study proves that the MEM is not only sensitive to the ND_3 orientation in the case of potassium–ammonia intercalated graphite but provides direct evidence of its orientation. The simplicity and versatility of this approach as shown in the case of stage 3 $MoCl_5$-GIC should ensure its applicability to a wide range of oriented layered systems.

The authors thank M. Suzuki for kindly providing an $MoCl_5$-GIC sample. This work was supported in part by NATO grant number CRG 910916.

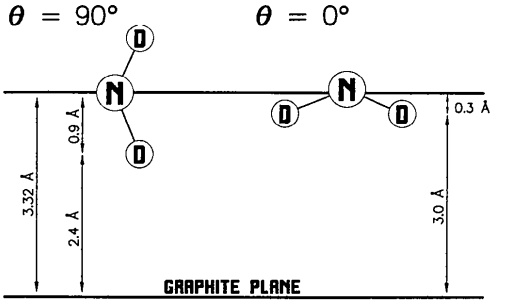

Fig. 6. Positions of the atoms of the ammonia molecule with respect to the graphite basal plane ($z = 0$) with the ammonia threefold axis lying in plane ($\theta = 90°$) and normal to the basal plane ($\theta = 0°$).

References

BRICOGNE, G. (1984). *Acta Cryst.* A**40**, 410–445.
FAN, Y. B., SOLIN, S. A., NEUMANN, D. A., ZABEL, H. & RUSH, J. J. (1987). *Phys Rev. B*, **36**, 3386–3393.
FRIEDEN, B. R. (1972). *J. Opt. Soc. Am.* **62**, 511–518.
JAYNES, E. T. (1957). *Phys. Rev.* **106**, 620–630; **108**, 171–190.
NEUMANN, D. A., ZABEL, H., FAN, Y. B., SOLIN, S. A. & RUSH, J. J. (1988). *Phys. Rev. B*, **37**, 8424–8431.
NEUMANN, D. A., ZABEL, H., RUSH, J. J., FAN, Y. B. & SOLIN, S. A. (1987). *Phys. Rev. C*, **20**, L761–764.
PRINCE, E. (1989). *Acta Cryst.* A**45**, 200–203.
QIAN, X. W., STUMP, D. R. & SOLIN, S. A. (1986). *Phys. Rev. Lett.* **33**, 5756–5768.
QIAN, X. W., STUMP, D. R., YORK, B. R. & SOLIN, S. A. (1985). *Phys. Rev. Lett.* **54**, 1271–1274.
SUZUKI, M., FURUKAWA, A., IKEDA, H. & NAGANO, H. (1983). *J. Phys. C*, **16**, 1211–1215.
SUZUKI, M., SANTODONATO, L. J., SUZUKI, I. S., WHITE, B. E. & COTTS, E. J. (1991). *Phys. Rev. B*, **43**, 5805–5814.

Acta Cryst. (1993). B**49**, 158–164

Structures of the Lovozerite Type – a Quantitative Investigation

BY YU. A. MALINOVSKY

Institute of Crystallography, Leninsky pr. 59, 117333 *Moscow, Russia*

AND H. BURZLAFF AND W. ROTHAMMEL

Lehrstuhl für Kristallographie, Institut für Angewandte Physik, Bismarckstr. 10, *D*-8520 *Erlangen, Germany*

(*Received* 2 *March* 1992; *accepted* 18 *June* 1992)

Abstract

The structure of lovozerite is derived from perovskite. For 24 members of the lovozerite family an aristotype is postulated. The method of quantitative comparison using the concept of mappings is applied to the lovozerite family using the aristotype as a 'structural unit'. The method is extended to relationships of symmetry-type II, *i.e.* the derived structure and the aristotype have only a common subgroup, the remaining non-common symmetry of the derived structure is used as 'distribution' symmetry for the structural unit. The numerical results are discussed in detail.

Introduction

Lovozerite is a silicate structure with the general composition $M1M2_2M3_3M4_3$ $[Si_6O_{18}]$ where $M1$, $M2$, $M3$, $M4$ are different metals and Si_6O_{18} represents a chair-form ring silicate group. The compounds either occur as minerals or they may be synthetic. Details are given in Tables 3 and 4.

Recently one of the authors of the present work (Tamazyan & Malinovsky, 1990) showed that the structure of lovozerite can be regarded as a structural unit or motive which can be found in a series of different structures thus defining the lovozerite family. It was recognized that the structural unit will be repeated by translations, centres of symmetry, different screw and rotation axes and glide planes; the symmetry operations used for the repetition may be regarded as 'distribution' symmetry.

In addition, the other two authors (Burzlaff & Rothammel, 1992) proved that structural relations can be described by application of the concept of mappings: a pair of matrices (**A**, **S**) is used to map the lattices, the symmetry operations and the positions of the atoms of two related structures onto each other. This procedure gives rise to the introduction of 'figures of merit' that allow the degree of relationship to be characterized by numerical values. In the first step only those relations that use translations as distribution symmetry were discussed.

It is the intention of this paper to combine both ideas:

(i) the concept of mapping will be extended to structural relations with all types of distribution symmetry;

(ii) this procedure will be applied to structures of the lovozerite family.

Derivation of the lovozerite structure

The members of the lovozerite-type family which possess the highest symmetry occur in space group $R\bar{3}m$; it is convenient to use rhombohedral axes to describe the structure. The lovozerite structure may be derived from perovskite (*e.g.* $CaTiO_3$) with space group $Pm\bar{3}m$, Ca on 1(*a*) $m\bar{3}m$ (0, 0, 0), Ti on 1(*b*) $m\bar{3}m$ ($\frac{1}{2}$, $\frac{1}{2}$, $\frac{1}{2}$) and O on 3(*c*) 4/*mm.m* (0, $\frac{1}{2}$, $\frac{1}{2}$) (*cf.* Fig. 1*a*); eight unit cells of perovskite lead to a unit cell of lovozerite by doubling the lattice parameter of perovskite without any shift, small deviations from cubic metric occur with respect to the angles, α is

0108-7681/93/020153-07$06.00